REVISTA MATÉRIA V.31
ISSN 1517-7076 articles e20260210, 2026

Evaluation of methylene blue dye adsorption in the composite of babassu coconut biochar – bentonite

Rigoberto Soares do Nascimento[1], Rafaella da Silva Gomes Alves[1], Laryssa Coutinho da Silva[1], Pedro Queiros Santiago[1], Caio Victor Pereira Pascoal[1], Maria Alexsandra de Sousa Rios[1], Ricardo Emilio Ferreira Quevedo Nogueira[1]

[1]Universidade Federal do Ceará. Fortaleza, CE, Brasil.

e-mail: rigobertoartigo@gmail.com, rafaellaalves719@gmail.com, laryssacoutinho@alu.ufc.br, pedroqueiros@alu.ufc.br, caiovictorppascoal@gmail.com, alexsandrarios@ufc.br, emilio@ufc.br

ABSTRACT

Adsorption is an effective and low-cost technique for dye removal from wastewater, motivating the development of sustainable adsorbent materials. However, studies on biochar–bentonite composites derived from babassu coconut shell (*Attalea speciosa*) remain limited. This study systematically investigated, for the first time, the influence of pyrolysis temperature on the physicochemical, structural, thermal, and adsorption properties of babassu shell biochar–bentonite composites for methylene blue removal. Biochars were produced at 350, 450, and 550 °C, and composites containing 5 wt% bentonite were characterized by FTIR, XRD, SEM/EDS, and TGA/DTG. Increasing the pyrolysis temperature promoted carbonization, aromatic condensation, and thermal stability, while bentonite incorporation preserved the smectite structure, improved mineral dispersion, and enhanced the structural stability of the composites. Adsorption performance increased with both pyrolysis temperature and adsorbent dosage, with BC550-5B exhibiting the highest adsorption capacity (73.89 mg/g). Equilibrium data were best fitted by the Langmuir model (R^2 = 0.975). In contrast, kinetic analyses showed that BC550 followed the PFO model, and BC550-5B was better described by the PSO model, indicating the contribution of heterogeneous active sites introduced by bentonite. These findings demonstrate that pyrolysis temperature and mineral modification act synergistically to produce efficient, potentially cost-effective, and sustainable adsorbents for wastewater treatment.

Keywords: Babassu coconut; Adsorption; Methylene blue; Composite; Waste management.

1. INTRODUCTION

The discharge of dye-containing effluents from textile, pharmaceutical, paper, and related industries has become a major environmental concern due to the persistence, toxicity, and low biodegradability of many synthetic dyes. Conventional treatment technologies, including coagulation, oxidation, membrane filtration, and biological processes, often present limitations related to operational cost, sludge generation, or reduced efficiency for recalcitrant contaminants [1]. Consequently, adsorption has emerged as one of the most effective and economically viable approaches for dye removal because it can efficiently remove pollutants even at low concentrations, does not generate large volumes of secondary sludge, requires relatively simple operation, and allows the use of inexpensive and renewable adsorbent materials. These advantages make adsorption particularly attractive for treating recalcitrant dye-containing effluents compared with many conventional physicochemical and biological treatment methods [1, 2].

Among the adsorbent materials investigated in recent years, biochar has received considerable attention due to its low production cost, environmental sustainability, and advantageous physicochemical properties. Its adsorption performance is strongly influenced by feedstock characteristics and pyrolysis conditions, which can modify aromaticity, surface functionality, structural organization, and depending on the production conditions, surface area and porosity [3]. Numerous studies have reported the use of agricultural residues such as rice husks, coconut shells, sawdust, corn straw, and sugarcane bagasse for biochar production. More recently, biomass derived biochars have also attracted increasing attention for the removal of emerging contaminants such as microplastics from aquatic environments. Their porous structure, abundant surface functional groups, and

Corresponding Author: Maria Alexsandra de Sousa Rios Received on 08/03/2026 Accepted on 24/08/2026

DOI: https://doi.org/10.1590/1517-7076-RMAT-2026-0210

(cc) BY

hydrophobic domains promote interactions with polymer particles through electrostatic attraction, pore filling, hydrophobic interactions, and π–π interactions, highlighting the versatility of biochar as a sustainable adsorbent for different classes of water pollutants. However, the search for alternative biomass sources remains important because feedstock composition directly influences the physicochemical properties and adsorption performance of the resulting material [3, 4].

Babassu coconut shell (*Attalea speciosa*) is an abundant agroindustrial residue in Brazil, particularly in the North and Northeast regions, where large quantities are generated annually and often are underutilized. Compared with many conventional lignocellulosic feedstocks, babassu shell presents high lignin content, elevated fixed-carbon yield, and remarkable mechanical resistance, characteristics that favor the formation of highly aromatic and thermally stable biochars [5]. Previous studies have demonstrated the potential of babassu-derived biochars for environmental applications; however, most investigations have focused on pristine biochars, while modifications aimed at improving adsorption performance remain relatively unexplored.

In parallel, clay minerals have been widely investigated as adsorbent materials because of their natural abundance, low cost, chemical stability, and ion-exchange properties. Among them, bentonite is particularly attractive due to its predominance of montmorillonite, a smectite mineral characterized by a layered aluminosilicate structure, high specific surface area, and significant cation exchange capacity [6, 7]. These properties are highly advantageous because they allow for efficient interactions with contaminants through electrostatic attraction, ion exchange, and surface complexation. Nevertheless, pure bentonite may suffer from particle aggregation and limited accessibility of active sites, restricting its adsorption performance under certain conditions [7, 8].

To overcome these limitations, the development of biochar–bentonite composites has emerged as a promising strategy. Recent studies have shown that combining biochar with bentonite can improve structural stability, increase the availability of adsorption sites, enhance thermal resistance, and promote synergistic interactions between the carbonaceous and mineral phases [9, 10]. For example, COUTINHO DA SILVA *et al*. [4] reported enhanced adsorption performance of ball–milled biochar–bentonite composites due to increased surface area and improved dispersion of mineral phases. HARINDINTWALI *et al*. [11] highlighted, through a meta-analysis, that physicochemical modifications of biochar significantly improve contaminant removal from water by increasing the availability of active adsorption sites. More recently, SHAKIR and AL-YAQOOBI [12] reported that bentonite-based biochar composites exhibited superior adsorption efficiency compared with pristine biochar owing to the complementary physicochemical properties of the mineral and carbonaceous phases. Despite the growing number of studies on biochar and bentonite-based composites, the literature remains largely focused on raw materials such as rice husks, sewage sludge and other agricultural residues. And systematic investigations addressing the influence of pyrolysis temperature on the physicochemical properties, thermal stability, and methylene blue adsorption performance of babassu shell-derived biochar–bentonite composites are still scarce [13, 14].

As a representative environmental contaminant, methylene blue (MB) is frequently used as a model pollutant in adsorption studies due to its chemical stability, well-defined molecular structure, and reliable spectroscopic detection. Its persistence in aquatic environments contributes to water coloration, limits light penetration, disrupts photosynthetic processes, and may cause toxic effects on aquatic organisms when discharged without adequate treatment [7, 15]. Being a cationic dye, MB readily interacts with carbonaceous and mineral surfaces through electrostatic attraction, hydrogen bonding, and π–π interactions, making it suitable for evaluating the adsorption performance of newly developed materials [16].

As summarized in Table 1, recent studies have demonstrated the potential of biochar–bentonite and related biochar–clay systems for removing different contaminants, but substantial differences remain in feedstock, mineral modification, preparation route, and target pollutant. Biochar–bentonite composites have been investigated using feedstocks such as macroalgae and sawdust, while babassu-derived adsorbents have predominantly been studied as pristine or chemically modified biochars rather than as biochar–bentonite composites. For example, SEWU *et al*. [6] employed macroalgae–bentonite composites for dye removal, whereas CHANDRASEKAR *et al*. [17] investigated a sawdust biochar-urea-bentonite system for methylene blue adsorption. Studies using babassu biomass have reported MB adsorption capacities of 67.6 mg/g for mesocarp-derived biochar and up to 387.5 mg/g for chemically modified babassu mesocarp, but these systems differ substantially from the composite formulation and preparation strategy investigated here.

To the best of our knowledge, the systematic effect of pyrolysis temperature on babassu endocarp biochar–bentonite composites for methylene blue adsorption has not yet been established. Accordingly, this study aims to investigate the effect of pyrolysis temperature on babassu endocarp biochar–bentonite composites containing 5 wt% bentonite for methylene blue removal. Biochars were produced at 350, 450, and 550 °C, and the resulting materials were evaluated in terms of their structural, chemical, morphological, and thermal

Table 1: Comparison of previous studies on biochar–bentonite composites and babassu-derived biochars for methylene blue adsorption.

STUDY	FEEDSTOCK	PYROLYSIS TEMPERATURE	COMPOSITE (MINERAL %)	TARGET POLLUTANT	ADSORPTION CAPACITY	CHARACTERIZATION TECHNIQUES
COUTINHO DA SILVA *et al.*, 2026 [4], *ACS Omega*	Carnauba straw (*Copernicia prunifera*)	25 to 550°C (rate of 10°C/min)	N/A	Methylene Blue (MB)	CSB (255,70 mg/g) DCSB (328, 13 mg/g)	XRD; SEM-EDS; CHNS/O elemental; FTIR; TGA/DTG/ DTA
SANTIAGO *et al.*, 2026 [18], *Processes*	Carnauba stalk (*Copernicia prunifera*)	25 to 550°C (rate of 10°C/min)	N/A	Methylene Blue (MB)	SB (210.7 mg/g)	XRD; SEM-EDS; CHNS/O elemental; FTIR; TGA/DTG/ DTA
SEWU *et al.*, 2019 [6], *J. Taiwan Inst. Chem. Eng.*	Macroalgae (*Saccharina japonica*) + Bentonite	600°C for 1 hour at a rate of 10°C/min	5%, 10%, and 20% bentonite	Congo Red (CR) and Crystal Violet (CV)	KBC-B5co (CV at 1275 mg/g)	BET; SEM-EDS; CHNS/O elemental; ICP-OES; FTIR; TGA
CHANDRASEKAR *et al.*, 2024 [17], *Environmental Research*	Urea + Bentonite + Biochar (from Sawdust)	500°C for 90 minutes (heating rate of 10 °C/min)	Biochar: Urea: Bentonite (2:2:1 mass ratio)	Methylene blue (MB) and Direct blue-6 (DB-6)	MB (53.17 mg/g) Direct blue-6 (41.33 mg/g)	FESEM; EDS; XRD; Raman spectroscopy; FTIR; XPS; BET; DLS
RAMOLA *et al.*, 2020 [8], *Sci. Total Environ.*	Bentonite + Calcite + Biochar	300°C, 500°C, and 700°C for 90 min (heating rate of 15°C/h)	bentonite or calcite in a 5:1 ratio (w/w)	Lead (Pb)	CCS 700 (160.85 mg/g) BCS 700 (101.86 mg/g)	TGA; SSA; FT-IR; XRD; SEM-EDS
SHAKIR and AL-YAQOOBI, 2025 [12], *Int. J. Renewable Energy Dev.*	Biochar (*Dodonaea viscosa*) + Bentonite + Boric Acid	Microwave-assisted pyrolysis in a 130 W reactor for 15 minutes	Bentonite: Biochar (1:1 mass ratio)	Pinoxaden (herbicide)	BBBC (130 mg/g)	SEM; EDX; BET; XRD; FTIR
DING *et al.*, 2016 [19], *J. Ind. Eng. Chem.*	Hickory wood + NaOH + HNO_3	350°C, 450°C, and 600°C for 5 h, 3 h and 2 h (rate of 20°C/min)	N/A	Lead [Pb (II)]	Pb (II) ranged from 12.2 to 16.3 mg/g	SEM; ICP-OES; FT-IR; XRD; XPS; TG/DTG; Zeta Potential; BET
CONSIGLIO KASEMODEL *et al.*, 2024 [15], *Int. J. Environ. Sci. Technol.*	Babassu coconut mesocarp (*Orbignya speciosa*)	N/A	N/A	Methylene Blue (MB)	MB (67.6 mg/g)	FTIR; BET; TGA; pH; EC; Proximate Analysis
VIEIRA *et al.*, 2011 [20], *Chem. Eng. J.*	Babassu (*Orbignya speciosa*) epicarp	N/A	N/A	Blue Remazol 160; Ruby S2G; Red Remazol 5 R; Brilliant Violet Remazol 5R; Indanthrene Olive Green	BR 160 (6.98 mg/g); VR 5 (4.58 mg/g); RR 5 (4.25 mg/g); R S2G (9.19 mg/g); IOG (1430 mg/g)	FTIR; BET; pHPZC; UV-Vis Spectroscopy
DA SILVA LIMA *et al.*, 2023 [5], *J. Phys. Chem. Solids*	Babassu mesocarp (*Orbignya speciosa*)+ KOH + NaOH + NaCl + HCl	110°C and 600 °C for 1 hour (heating rate of 30°C/min)	Biochar: Hydroxide (1:2 | 4:3 | 4:3 mass ratio)	Methylene Blue (MB) and Crystal Violet (CV)	AC-4 (387.5 mg/g) AC-3 (292.0 mg/g) AC-1 (240.0 mg/g) AC-2 (89.5 mg/g)	CHNS analysis; FTIR; XRD; TGA; XPS; SEM; TEM
Present study	Babassu endocarp (*Attalea speciosa*)	350°C, 450°C and 550°C for 1 hour (rate of 25°C/min)	5 wt% bentonite	Methylene Blue (MB)	73.89 (BC550-5B)	FTIR; XRD; SEM/EDS; TGA/DTG; UV-Vis

(cc) BY

characteristics and adsorption performance. By maintaining the bentonite loading constant while varying the pyrolysis temperature, this study provides a controlled assessment of the relationship between carbonization conditions, composite properties, and methylene blue adsorption. The study therefore contributes to the development of sustainable adsorbents by combining the valorization of an underutilized Brazilian agroindustrial residue with mineral modification and provides experimental evidence for identifying suitable preparation conditions for methylene blue adsorption.

2. MATERIALS AND METHODS

This section describes the materials used, the preparation procedures for the biochar and biochar–bentonite composites, the physicochemical characterization techniques, and the adsorption experiments performed to evaluate the removal of methylene blue. The experimental methodology was designed to ensure the reproducibility of the preparation process and to establish relationships between the physicochemical properties of the materials and their adsorption performance.

2.1. Preparation of the biochar and biochar−bentonite composite

The carbonaceous precursor was the endocarp of the babassu coconut (Attalea speciosa), collected in São Luís, Maranhão, Brazil (geographic coordinates: 2°31′51″ S; 44°18′24″ W), under SISGEN code A6B2232. The biomass was initially crushed in a knife mill (Simple Centrifugal Mill − MCS 280-5cv) to obtain a homogenous particle size. Then, the biomass was carbonized in a muffle furnace (QUIMIS Q31M) at three different temperatures (350, 450, and 550 °C) using a heating rate of 25 °C·min^{-1} and a residence time of 1 hour. The pyrolysis was carried out under self-generated oxygen-limited conditions at atmospheric pressure, without an external inert gas flow. Under these conditions, the restricted oxygen availability inside the closed crucibles promoted the thermochemical conversion of the biomass while minimizing oxidative degradation. The resulting biochars were designated as BC350, BC450, and BC550.

Composites were prepared using bentonite clay from Pedra Lavrada, Paraíba, Brazil (geographic coordinates: 6°45′25″ S; 36°28′48″ W) incorporated into the biochar samples at a proportion of 5 wt%. This mineral loading was selected based on previous studies reporting enhanced adsorption performance at this proportion [21]. The composites were designated as BC350−5B, BC450−5B, and BC550−5B.

2.2. Characterization

Surface morphology was analyzed by SEM (Hitachi TM3000, Japan, 15kV), with elemental composition determined by EDS (Swift ED3000, Oxford Instruments, UK). Crystalline phases were identified by XRD (PANalytical X'Pert PRO, Co−Kα radiation, 2θ = 3−100°). Functional groups were evaluated by FTIR (Bruker VERTEX 70v, ATR mode, 4000−380 cm^{-1}, 2 cm^{-1} resolution). Thermal stability was assessed by TGA (TA Instruments Q50) from room temperature to 800 °C at 10 °C·min^{-1} under controlled gas flow. UV−Vis analyses were performed using an SP 2000 spectrophotometer (Spectrum, China) in the 600−700 nm range.

2.3. Methylene blue adsorption tests

A stock solution of methylene blue ($C_{16}H_{18}ClN_3S$) was prepared (1 g/L) using analytical-grade dye (Synth Chemical Products, 95% purity) and deionized water. Batch adsorption experiments were carried out at 25 °C under orbital agitation (80 rpm) and pH = 6.35. A total volume of 100 mL of methylene blue solutions with initial concentrations ranging from 250 to 1000 mg/L was contacted with adsorbent dosages of 4–10% (w/v). All adsorption experiments were performed in quadruplicate, and the results are presented as mean values. After 1 hour of agitation, the suspensions were filtered, and the residual dye concentration was determined using a UV–Vis spectrophotometer (SP 2000 UV−Spectro, LanGAT, Unicentro, Brazil) at 664 nm. The methylene blue concentration was determined using an external calibration curve (0.5–2 mg/L), which exhibited excellent linearity (Figure A1), with the corresponding linear regression equation and coefficient of determination (R^2) provided in the Appendix. Although international organizations such as the WHO do not establish a specific drinking-water guideline value for methylene blue, its persistence and potential ecotoxicological effects justify the development of efficient removal technologies before wastewater discharge.

The dye removal efficiency (R%) was calculated according to Equation (1) [22]:

$$R(\%) = \left(\frac{C_o - C_e}{C_o}\right) \times 100 \quad (1)$$

Where C_o and C_e (mg/L) are, respectively, the initial and equilibrium dye concentrations, and R (%) is the removal efficiency.

The adsorption capacity at equilibrium (q_e, mg/g) was calculated as [23]:

$$q_e = \frac{(C_o - C_e)V}{m} \tag{2}$$

Where V (L) is the solution volume and m (g) is the adsorbent mass.

Equilibrium data were fitted to the Langmuir and the Freundlich isotherm models in their non-linear forms. The Langmuir model is described in non-linear form by Equation (3) [23]:

$$q_e = \frac{q_{max} K_L C_e}{1 + K_L C_e} \tag{3}$$

Where q_e (mg/g) is the amount of dye adsorbed per unit mass of adsorbent; q_{max} (mg/g) is the maximum adsorption capacity; K_L (L/mg) is the Langmuir constant, and C_e (mg/L) is the equilibrium dye concentration in solution.

The Freundlich is described in its non-linear form by Equation (4) [18]:

$$q_e = K_F C_e^{\frac{1}{n}} \tag{4}$$

Where q_e (mg/g) is the amount of dye adsorbed per unit mass of adsorbent; Ce (mg/L) is the equilibrium dye concentration in solution; K_F [(mg/g) (L/mg)$^{1/n}$] and 'n' are Freundlich constants associated with adsorption capacity and surface heterogeneity, respectively.

The pseudo-first order (PFO) kinetic model is described in its linearized form by Equation (5) [18]:

$$ln\,(q_e - q_t) = ln\,(q_e) - k_1 t \tag{5}$$

Where q_e (mg/g) is the amount of dye adsorbed per unit mass of adsorbent; q_t (mg/g) are the amounts of adsorbate adsorbed per gram of adsorbent at time *t*; k_1 (min^{-1}) is the PFO rate constant.

The pseudo-second order (PSO) kinetic model is described in its linearized form by Equation (6) [18]:

$$\frac{1}{q_t} = \frac{1}{k_2 q_e^2} + \frac{t}{q_e} \tag{6}$$

Where q_e (mg/g) is the amount of dye adsorbed per unit mass of adsorbent; q_t (mg/g) are the amounts of adsorbate adsorbed per gram of adsorbent at time *t*; k_2 (g/mg·min) is the PSO rate constant.

The practical applicability of the developed composites should be interpreted with caution because the adsorption experiments were conducted using synthetic methylene blue solutions. Real textile effluents present a considerably more complex matrix, containing mixtures of dyes, inorganic salts, surfactants, organic matter, and other dissolved species that may compete for adsorption sites or modify surface–adsorbate interactions. Consequently, the adsorption capacity obtained under controlled laboratory conditions may not directly represent the performance of BC550–5B in real wastewater. Validation using actual textile effluents and multicomponent solutions is therefore necessary to determine the influence of competing species and matrix effects on adsorption efficiency.

3. RESULTS AND DISCUSSION

This section presents and discusses the physicochemical characterization of the biochars and biochar–bentonite composites, together with their adsorption performance toward methylene blue. The effects of pyrolysis temperature and bentonite incorporation on the structural, thermal, morphological, and adsorption properties of the materials are examined to establish relationships between material characteristics and adsorption behavior.

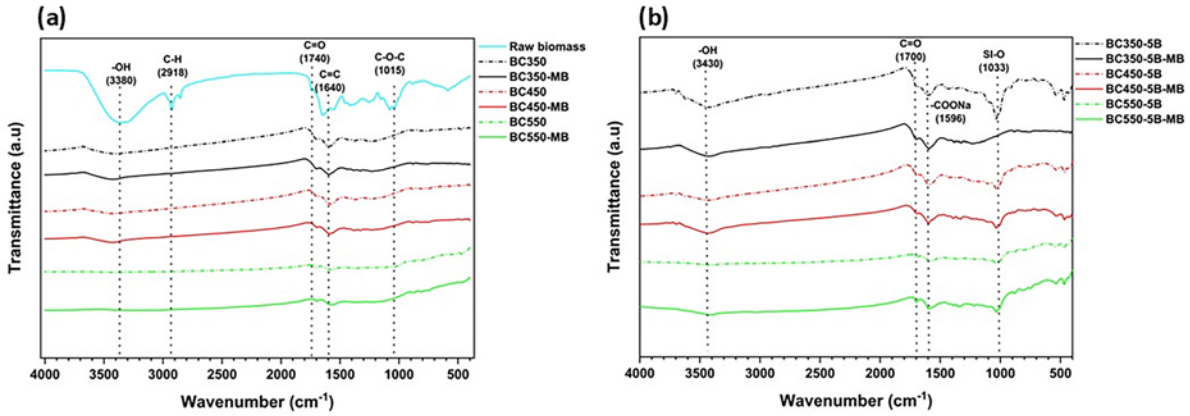


Figure 1: FTIR spectra of (a) raw biomass and biochars produced at 350, 450, and 550 °C (BC350, BC450, and BC550) before and after methylene blue adsorption and (b) biochar-bentonite composite prepared with 5% bentonite produced at 350, 450, and 550 °C (BC350-5B, BC450-5B, and BC550-5B) and the comparison of spectra before and after methylene blue adsorption.

3.1. Characterization of adsorbents

The particle size of the samples was homogenized using 200-mesh sieves. Functional groups and vibrational frequencies were identified by Fourier-transform infrared (FTIR) spectroscopy, and the corresponding spectra are presented in Figure 1.

The progressive reduction in intensity of O–H, C=O, and C–O bands with increasing pyrolysis temperature (Figure 1a) confirms the thermal decomposition of hemicellulose, cellulose, and lignin, as previously reported [4, 18]. This structural evolution is significant because it indicates that higher temperatures produce a more condensed aromatic framework, which is favorable for π–π interactions with aromatic dye molecules such as MB. The residual functional groups observed at 550 °C, although reduced in intensity, still provide sites for hydrogen bonding, contributing to the multifunctional adsorption mechanism of BC550. Consequently, the absorption bands associated with O–H stretching (~3380 cm^{-1}) [5], aliphatic C–H stretching (~2918 cm^{-1}) [24], C=O stretching of carboxyl, carbonyl, or ester groups (~1740 cm^{-1}) [24], aromatic C=C stretching (~1640 cm^{-1}) [25], and C–O stretching of alcohols, phenols, or ethers (~1015 cm^{-1}) [25] become less intense with increasing pyrolysis temperature. After adsorption, reductions and slight shifts in the intensity bands of the O–H, C=O, and C–O were observed, suggesting that these functional groups in the adsorption process occur through hydrogen bonding and electrostatic interactions. These spectral changes demonstrate that pyrolysis temperature plays a key role in controlling surface functionality and carbon structural development. Lower temperatures preserve more oxygenated functional groups, whereas higher temperatures promote aromatization and carbon condensation, directly influencing adsorption performance, as also reported by COUTINHO DA SILVA *et al*. [4].

Compared with the corresponding pristine biochars prepared at the same pyrolysis temperature, the composites exhibit the characteristic Si–O vibration of bentonite together with broader O–H absorption bands, confirming the successful incorporation of the clay phase into the carbon matrix [19, 26]. The coexistence of carbonaceous and aluminosilicate functional groups indicates that composite formation introduces additional surface functionalities while preserving the aromatic framework generated during pyrolysis, consistent with the observations of SANTIAGO *et al*. [18]. After adsorption, alterations in the intensity and position of O−H, C=O, and Si−O bands were detected, suggesting the participation of these functional groups in the binding of dye molecules through hydrogen bonding, electrostatic interactions, and π−π stacking with the aromatic domains of biochar [7, 22].

Figure 2 shows X-ray diffraction (XRD) was carried out to investigate how pyrolysis temperature influences carbon structural organization and to determine whether bentonite retains its layered crystalline structure after composite formation. A comparison of biochar and biochar–bentonite composites produced at identical temperatures also enables the distinction between structural changes associated with carbonization and those introduced by the mineral phase. Figure 2(a) shows that BC350, BC450, and BC550 exhibit predominantly amorphous patterns, characterized by broad halos centered at approximately $2\theta \approx 12°$ and 22−24°, which is typical of biochars with disordered carbon structure [22]. The broad hump near 24° corresponds to the (002) plane of turbostratic carbon, indicating poorly ordered graphitic domains. The absence of sharp, intense reflections confirms the low degree of crystallinity of the biochars [23].

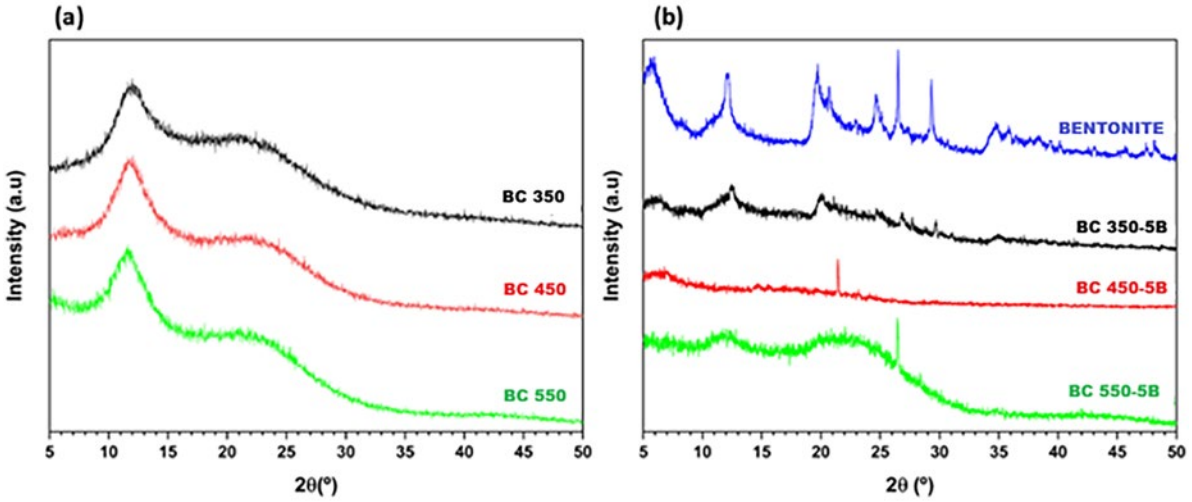


Figure 2: X-ray diffraction (XRD) patterns of (a) biochars produced at 350, 450, and 550 °C (BC350, BC450, and BC550) and (b) bentonite and biochar-bentonite composites prepared with 5% bentonite produced at 350, 450, and 550 °C (BC350-5B, BC450-5B, and BC550-5B).

Figure 2(b) shows that bentonite presents sharp reflections at approximately 2θ ≈ 5−6°, 12°, 19−20°, and 26°, corresponding to smectite/montmorillonite basal and higher-order planes. Secondary reflections near 26.6° and 29° are consistent with quartz (SiO_2) and calcite ($CaCO_3$), respectively [23]. In the biochar-bentonite composites, the basal reflection near ~ 6° is retained with reduced intensity, indicating partial preservation of the layered smectite structure after composite formation, a behavior also reported for montmorillonite-modified biochars. The decrease in intensity of reflections near 12° and 19° suggests structural modification of the clay layers or partial coverage by carbonaceous material, which is commonly observed in clay-biochar systems due to interaction between the carbon matrix and layered silicates [10, 23].

Furthermore, the coexistence of the amorphous carbon halo (~24°), characteristic of turbostratic carbon, together with well-defined clay reflections, supports the successful integration of montmorillonite within the biochar matrix, consistent with previously reported composite diffraction patterns. The slightly more defined peak near 26° in BC550-5B may be associated with quartz from the clay matrix or increased structural ordering of carbon domains at higher pyrolysis temperature [23, 27]. Overall, increasing pyrolysis temperature resulted in a slight increase in carbon structural ordering while preserving the predominantly amorphous nature of the biochars. In contrast, the simultaneous presence of turbostratic carbon and crystalline clay phases demonstrates that the composite combines the structural stability of bentonite with the porous carbon matrix generated during pyrolysis, which is advantageous for adsorption applications [23, 28]. These structural comparisons also supported the selection of the 550 °C material, since this condition provided the best compromise between carbon structural development, preservation of clay crystallinity, thermal stability, and adsorption performance.

Thermal behavior and stability of the babassu-derived biochars and their bentonite composites were evaluated by TGA/DTG, (Figure 3), and the main thermal parameters are summarized in Table 2.

Thermograms 3(a) and 3(c) show three main mass-loss stages: (i) 25−210 °C, related to the removal of physically adsorbed moisture and light volatiles; (ii) 250−510 °C, associated with the decomposition of hemicellulose and cellulose; and (iii) 510−800 °C, attributed to lignin degradation and the progressive formation of stable aromatic carbon structures, leading to matrix stabilization [24, 29].

TGA results indicate that higher pyrolysis temperatures shift T_{onset} to higher values, confirming enhanced thermal stability due to increased carbonization and aromaticity. The same trend was observed for the 5% bentonite composites, with BC550-MB presenting the highest T_{onset} (326.46 °C), T_{offset} (547.89 °C), and greater residual mass, highlighting the contribution of the mineral phase. DTG curves support these findings: BC450 exhibited the highest degradation peak (435.1 °C), while BC550 showed a less intense peak, indicating a more condensed structure. The composite BC550-MB reached 504.2 °C, demonstrating delayed maximum degradation due to the barrier effect of bentonite's lamellar aluminosilicate structure [10, 23].

Scanning electron microscopy (SEM) images of bentonite and corresponding energy-dispersive X-ray spectroscopy (EDS) spectra are presented in Figure 4.

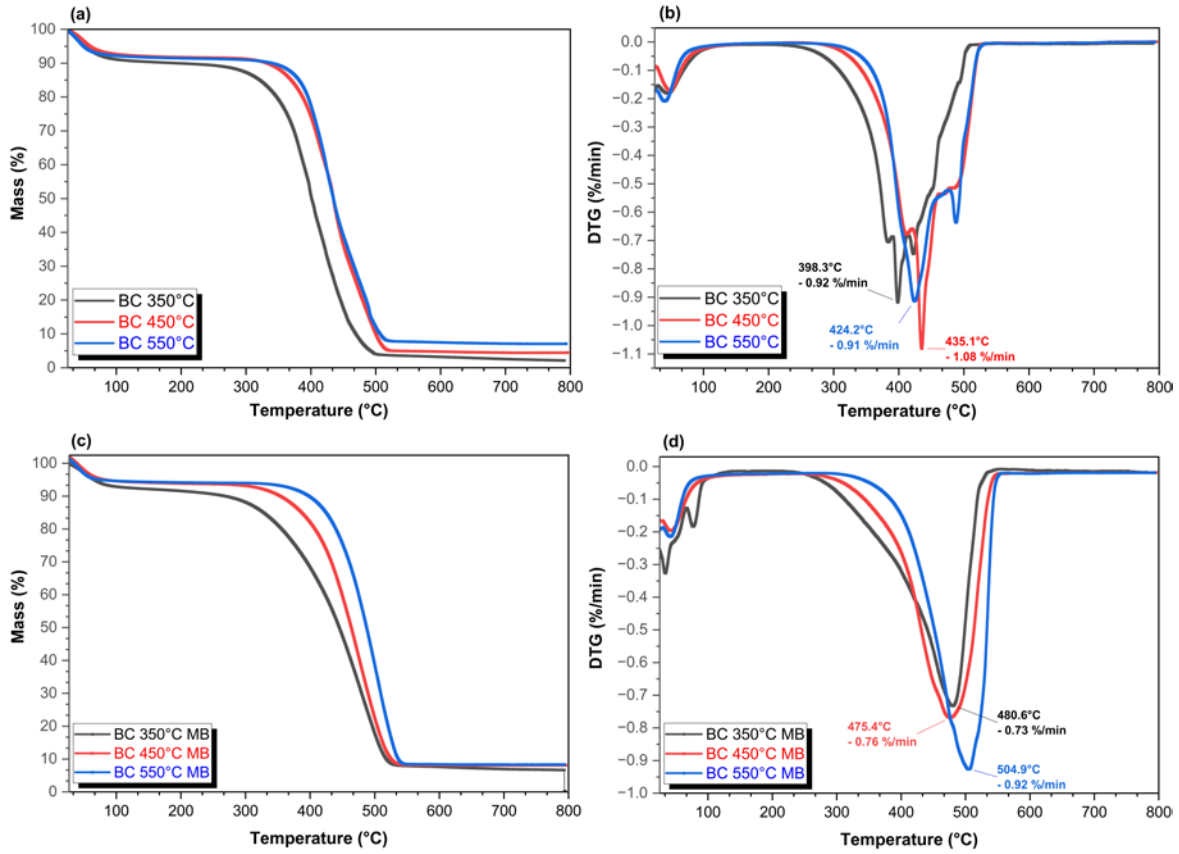


Figure 3: Thermograms of the materials under study: (a) TGA of biochars at 350°C, 450°C and 550°C; (b) DTG of biochars at 350°C, 450°C and 550°C; (c) TGA of composites (biochar + 5% bentonite) and (d) DTG of composites (biochar + 5% bentonite).

Table 2: Main thermal parameters obtained from TGA and DTG thermograms.

MATERIAL	SAMPLE	REGION I		REGION II		REGION III		RESIDUAL MASS (%)
		Δ[a]	T_{ONSET}[b]	Δ[a]	V_{MAX}[c]	Δ[a]	T_{OFFSET}[d]	
Biochar	BC 350	−10.73	255.38	−87.11	−0.92	−1.71	505.23	0.45
	BC 450	−08.45	297.48	−87.08	−1.08	−1.14	521.13	3.33
	BC 550	−09.15	309.87	−83.22	−0.91	−1.36	527.34	6.27
Composite	BC 350–MB	−07.46	218.72	−89.15	−0.73	−1.17	532.87	2.22
	BC 450–MB	−07.83	291.27	−80.39	−0.76	−0.89	541.74	10.89
	BC 550–MB	−08.14	326.46	−80.87	−0.92	−0.96	547.89	10.03

[a]Mass loss rate (in percentage).
[b]Onset temperature of maximum degradation (°C).
[c]Maximum reaction rates on DTG (%/min).
[d]Offset temperature of maximum degradation (°C).

The micrograph of the bentonitic clay, Figure 4(a) shows a typical smectite morphology, with lamellar, sheet-like particles arranged in irregular and partially compacted aggregates. The EDS spectrum confirms the typical elemental composition of bentonite, with O related to silica tetrahedra and hydrated octahedral sheets. The presence of Ca, Na, or K is attributed to isomorphic substitutions or exchangeable interlayer cations, responsible for swelling behavior and cation exchange capacity [7, 30]. This morphology is consistent with previous reports describing calcium bentonites as layered aluminosilicates with high ion-exchange potential, which favors their incorporation into biochar matrices and enhances adsorption performance [4, 18].

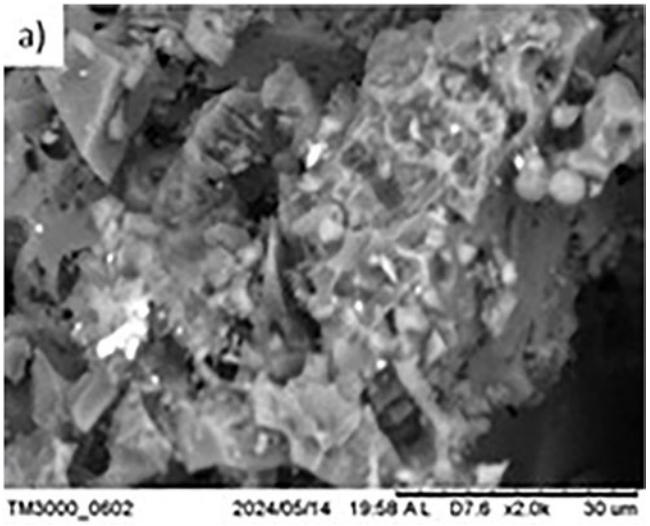


Figure 4: (a) MEV of bentonite.

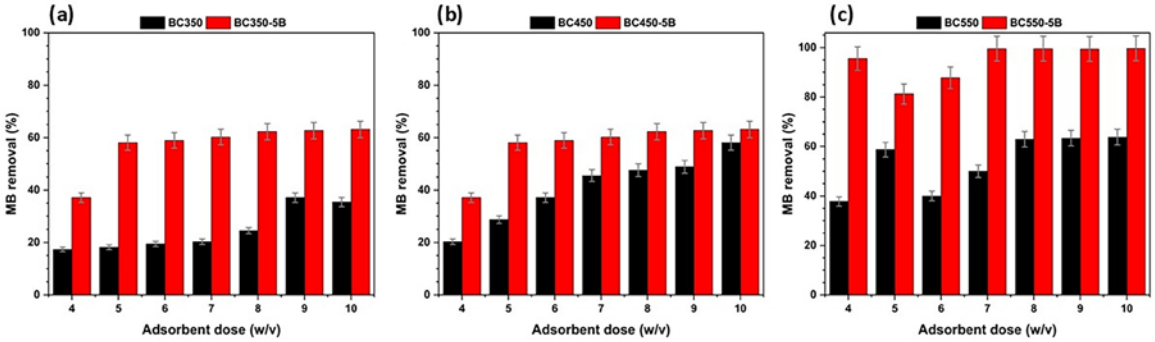


Figure 5: Adsorptive characteristics of biochar and composite, in the proportions of 4–10% (w/v), in a 1000 mg/L methylene blue solution: (a) BC350 and BC350-5B; (b) BC450 and BC450-5B; and (c) BC550 and BC550-5B.

3.2. Adsorption experiments

Figure 5 presents the effect of adsorbent dosage on dye removal at an initial concentration of 1000 mg/L. Adsorption efficiency increased with pyrolysis temperature for both biochar and biochar-bentonite composites. BC550 and BC550-5B showed the highest performance at all dosages, while 350 °C samples exhibited the lowest efficiencies.

This trend agrees with previous studies showing that higher pyrolysis temperatures significantly modify biochar properties. DING *et al*. [19] reported that increasing temperature from 300 to 600 °C raised carbon content and surface area while reducing O/C ratios and acidic groups, indicating greater carbonization. Similarly, MAHDI *et al*. [26] reported enhanced methylene blue adsorption for biochar produced at 550 °C and associated this behavior with changes in surface characteristics, porosity, and aromaticity.

Figures 6 and 7, further reveal the combined influence of adsorbent dosage and initial dye concentration. In general, higher dosages increased removal efficiency. For pristine biochar (Figure 6), the influence of pyrolysis temperature was more evident at higher dye concentrations (750 and 1000 mg/L), with BC550 outperforming BC350 and BC450. At lower concentrations (250 and 500 mg/L), differences among temperatures diminished at higher dosages, suggesting partial saturation of adsorption sites.

The incorporation of 5 wt% bentonite (Figure 7) significantly enhanced adsorption performance across most conditions. The improvement was particularly evident for materials produced at 550 °C, which achieved near-complete removal at intermediate dosages under lower dye concentrations (250−500 $mg \cdot L^{-1}$). This enhancement indicates a positive interaction between the mineral phase and the carbon matrix [5, 31].

(cc) BY

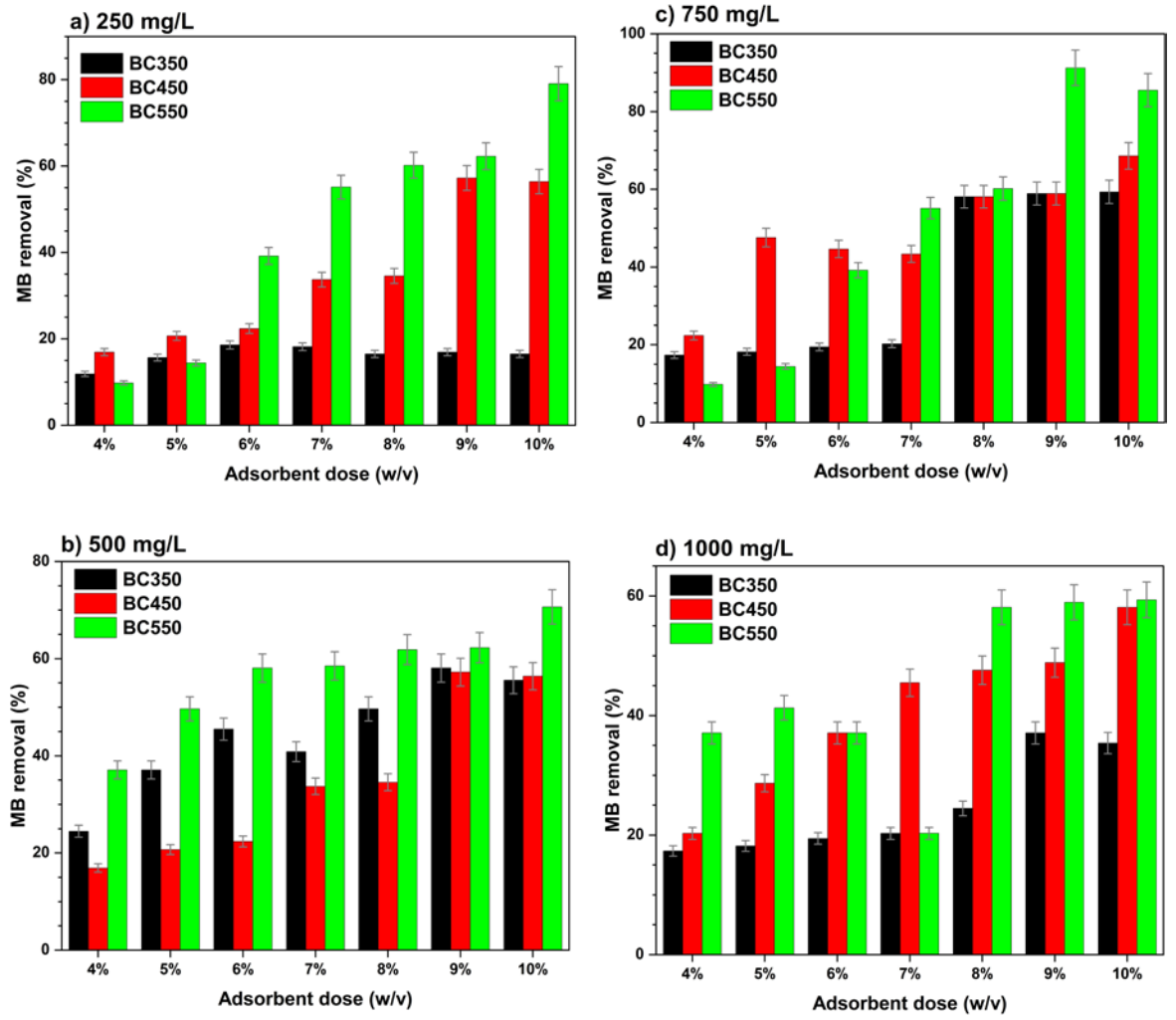


Figure 6: Adsorption efficiency of biochar, prepared at temperatures of 350, 450, and 550 °C, at (a) 250 mg/L, (b) 500 mg/L, (c) 750 mg/L and (d) 1000 mg/L methylene blue solution.

Interestingly, at lower temperatures (350 °C), the composite sometimes exhibited performance comparable to or slightly superior to the 450 °C material at lower dye concentrations, suggesting that mineral incorporation modifies the temperature-dependent adsorption behavior. At the highest dye concentration (1000 mg/L), overall efficiencies decreased due to the higher pollutant load. The superior adsorption performance observed for BC550 and BC550-5B can be attributed to the combined effects of increased carbonization and the presence of bentonite. Higher pyrolysis temperatures promote the development of a more aromatic carbon framework, greater structural stability, and improved accessibility of adsorption sites, while bentonite contributes additional negatively charged aluminosilicate surfaces capable of interacting with cationic methylene blue molecules through electrostatic attraction [7, 14]. In addition to electrostatic attraction, hydrogen bonding, and π–π interactions, pore filling and ion-exchange processes may also contribute to MB uptake [14]. Figure 8 presents a schematic illustration summarizing the proposed adsorption mechanisms of methylene blue on the biochar–bentonite composite.

Pore filling is plausible because pyrolysis promotes the development of a more carbonized and structurally condensed matrix, which may provide accessible porous domains for MB diffusion and retention [14]. However, the present TGA/DTG results provide evidence of thermal stabilization rather than direct confirmation of pore development or pore filling. The preserved smectite structure identified by XRD and the presence of exchangeable cations in the bentonite phase observed by SEM/EDS support the possible contribution of ion-exchange interactions between MB cations and the mineral surface.

Changes in the O–H, C=O, and Si–O bands after adsorption further indicate that surface functional groups may participate through hydrogen bonding and electrostatic interactions, while the increasingly aromatic carbon structure may favor π–π interactions with MB [12]. Surface complexation may also contribute to MB

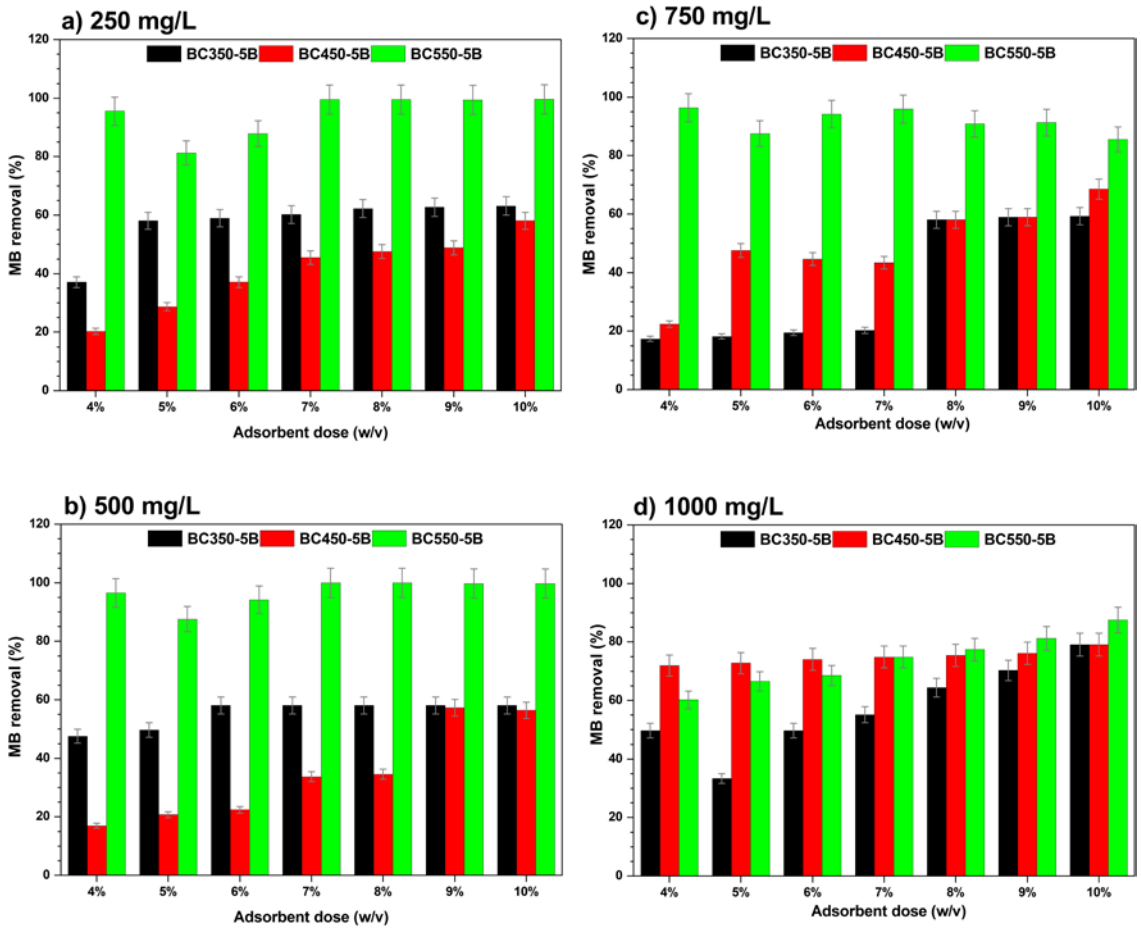


Figure 7: Adsorption efficiency of composite, prepared at temperatures of 350, 450, and 550 °C, at (a) 250 mg/L, (b) 500 mg/L, (c) 750 mg/L and (d) 1000 mg/L methylene blue solution.

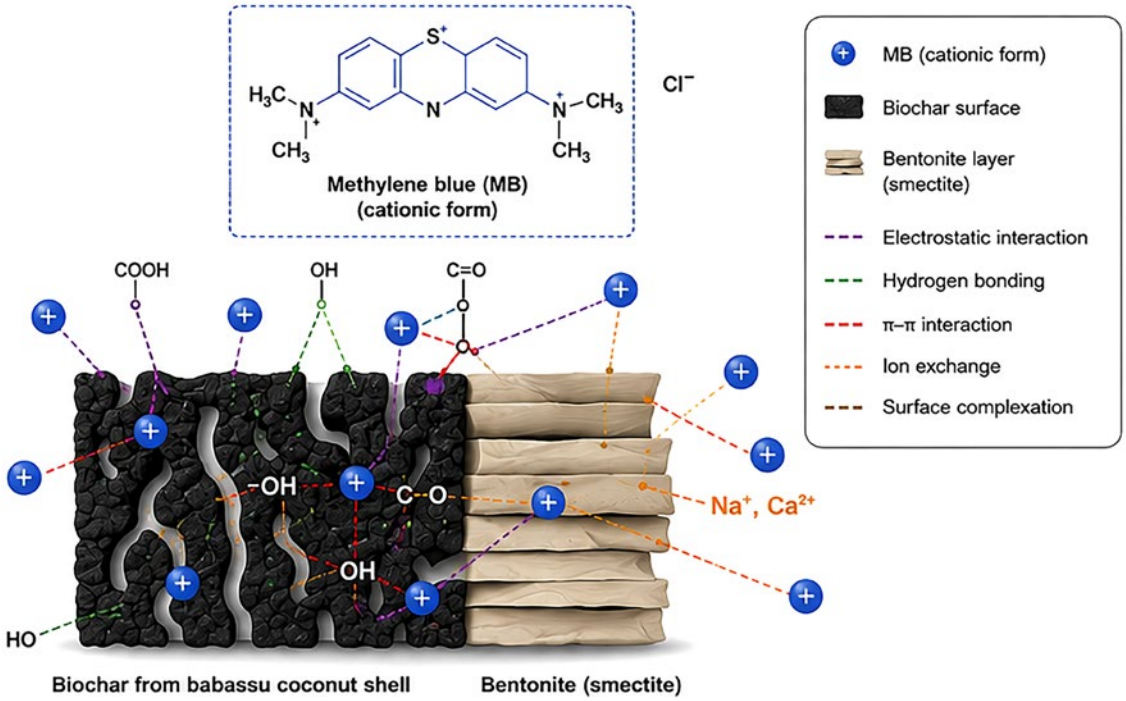


Figure 8: Schematic illustration of the proposed adsorption mechanisms of methylene blue (MB) on the babassu shell biochar–bentonite composite.

retention, but its occurrence cannot be confirmed from the present dataset. Direct techniques such as XPS, zeta potential measurements, BET analysis before and after adsorption, and pH dependent experiments would be required to distinguish and quantify the relative contribution of these mechanisms [12, 14].

The experimental and isotherm models for the adsorption of MB on the biochars with 5 wt% bentonite loading are shown in Figure 9, and the corresponding isotherm parameters are summarized in Table 3.

For the biochars (BC350, BC450, and BC550), the maximum adsorption capacity increased with pyrolysis temperature (Table 3). A similar influence of thermal treatment on MB adsorption performance was reported for

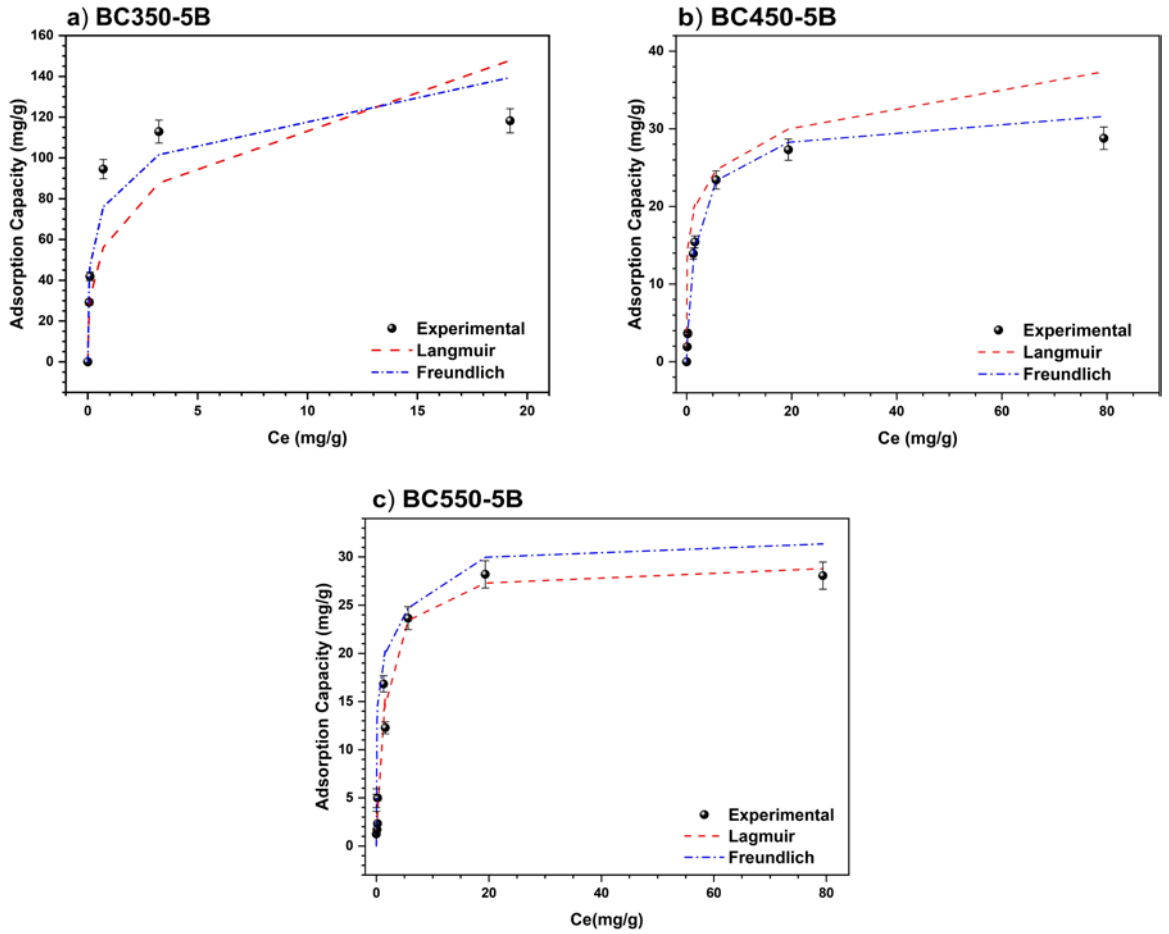


Figure 9: Experimental and Isotherm model for the adsorption of MB of (a) BC350-5B, (b) BC450-5B, and (c) BC550-5B.

Table 3: Parameters obtained from the Langmuir and the Freundlich models for the biochar samples.

ISOTHERM MODEL	PARAMETERS	BC350	BC350-5B	BC450	BC450-5B	BC550	BC550-5B
Langmuir	$q_{max}^{(a)}$	19.92 ± 1.21	45,13 ± 2.31	50,02 ± 1.89	59.44 ± 2.79	60,26 ± 0.91	73.89 ± 1.27
	$K_L^{(b)}$	0.706 ± 0.02	0.976 ± 0.04	0.310 ± 0.02	0.962 ± 0.04	0.814 ± 0.03	0.998 ± 0.01
	$R^{2(c)}$	0.918	0.916	0.962	0.975	0.978	0.975
Freundlich	$K_F^{(d)}$	18.86 ± 0.95	60.86 ± 3.20	19.15 ± 1.12	56.15 ± 1.82	20.74 ± 1.76	60.41 ± 2,89
	$n^{(e)}$	5.27 ± 0.22	6.31 ± 0.33	6.40 ± 0.28	6.77 ± 0.36	7.06 ± 0.29	8.40 ± 0.43
	$R^{2(c)}$	0.805	0.805	0.957	0.957	0.970	0.980

[a]Maximum adsorption capacity (mg/g).
[b]Adsorption equilibrium constant (L/mg).
[c]Coefficient of determination (dimensionless).
[d]Freundlich constant ((mg/g) (L/mg)$^{1/n}$).
[e]Heterogeneity factor (dimensionless).

babassu mesocarp biochar, where adsorption capacity varied according to processing conditions [15]. The Langmuir model provided the best overall description of the equilibrium data, particularly for BC450, BC450-5B, BC550, and BC550-5B (R^2 = 0.962–0.978), suggesting that adsorption predominantly occurred through monolayer coverage on relatively homogeneous active sites. In contrast, the lower correlation coefficients obtained for BC350 indicate greater surface heterogeneity, consistent with the lower degree of carbonization observed for the material. Freundlich constants (n = 5.27–8.40) remained higher than unity for all samples, indicating favorable adsorption over the investigated concentration range and confirming that the adsorption process became progressively more favorable with increasing pyrolysis temperature and bentonite incorporation.

The maximum adsorption capacity (q_{max}) obtained for BC550-5B (73.89 mg/g) is comparable or superior to several biochar-based adsorbents recently reported in the literature (Table 1). For instance, it exceeds the values reported for pristine babassu mesocarp biochar (67.6 mg/g) and sawdust-derived biochar-urea-bentonite composites (53.17 mg/g). While the chemically activated babassu materials reached higher capacities (up to 387.5 mg/g), the composite developed in this study offers a simpler and more cost-effective preparation route, which is advantageous for large-scale applications.

The adsorption capacities obtained in this study are comparable to values reported for other lignocellulosic biochars and biochar–bentonite composites employed for methylene blue removal under similar experimental conditions. Recent investigations have likewise reported that increasing pyrolysis temperature can enhance adsorption performance through changes in aromaticity, surface functionality, structural stability, and, in some systems, pore development; whereas bentonite incorporation provides complementary adsorption sites and improves the overall affinity toward cationic dyes [12, 32]. The synergistic effect of pyrolysis temperature and bentonite incorporation is evident when comparing the adsorption capacities of the materials: the maximum capacity increased from 19.92 mg/g (BC350) to 73.89 mg/g (BC550-5B) (Table 3). The approximately 3.7-fold increase in q_{max} from BC350 to BC550-5B indicates that the adsorption improvement cannot be attributed to pyrolysis temperature alone. Rather, the results suggest a combined contribution of progressive carbonization and the introduction of aluminosilicate adsorption domains by bentonite. This interpretation is supported by the FTIR, XRD, SEM/EDS, equilibrium, and kinetic results, although the individual contribution of each mechanism cannot be quantitatively isolated from the present dataset.

The adsorption mechanisms proposed in this study are supported by the combined characterization and equilibrium results; however, their relative contributions cannot be quantitatively distinguished from the present dataset. In particular, BET surface area and pore-size distribution measurements were not performed. Therefore, the enhanced adsorption observed with increasing pyrolysis temperature cannot be attributed solely to increased surface area or porosity. Instead, improvement is interpreted as the combined effect of increased carbonization, aromatic structural development, surface functionality, and bentonite incorporation. Complementary analyses, including BET, pore-size distribution, zeta potential, XPS, and pH-dependent adsorption experiments, would provide further evidence for distinguishing the contribution of these factors.

Adsorption kinetics were additionally evaluated for the best-performing biochar (BC550) and biochar–bentonite composite (BC550–5B), and the corresponding experimental data together with the pseudo-first order (PFO) and pseudo-second order (PSO) fittings are presented in Figure 10, while the kinetic parameters are summarized in Table 4. As shown in Figure 10(a), BC550 reached adsorption equilibrium after approximately 40 min, whereas BC550–5B required about 120–140 min to attain equilibrium (Figure 10(b)), indicating that the

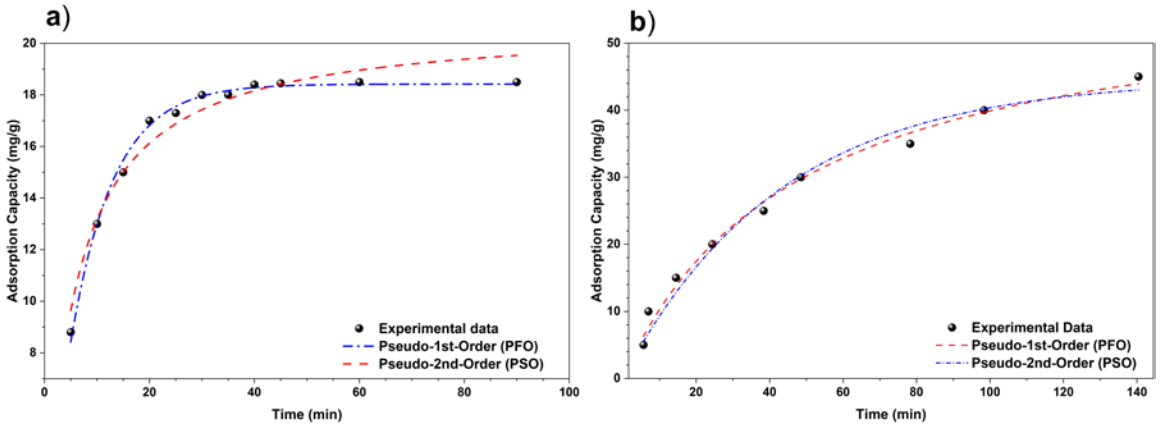


Figure 10: Experimental, PFO, and PSO models for the adsorption of MB of (a) BC550 and (b) BC550-5B.

Table 4: Parameters obtained from the PFO and PSO models for the biochar samples.

ISOTHERM MODEL	PARAMETERS	BC550	BC550-5B
Pseudo-First Order (PFO)	q_e [a]	18.42 ± 0.10	44.74 ± 2.13
	K_1 [b]	0.122 ± 0.03	0.023 ± 0.03
	R^2 [c]	0.993	0.978
Pseudo-Second Order (PFO)	q_e [a]	20.79 ± 0.44	58.79 ± 2.91
	K_2 [d]	$8.320 \cdot 10^{-3}$ ± 0.001	$0.359 \cdot 10^{-3}$ ± 0.001
	R^2 [c]	0.964	0.988

[a]Equilibrium adsorption capacity (mg/g).
[b]Pseudo-first order rate constant (h^{-1}).
[c]Coefficient of determination (dimensionless).
[d]Pseudo-second order rate constant (h^{-1}).

incorporation of bentonite increased the overall adsorption capacity while slightly slowing the adsorption rate due to the progressive occupation of a larger number of available adsorption sites. Similar behavior has been reported for biochar–bentonite composites, in which mineral incorporation increases the number of active sites but may prolong the time required to reach equilibrium because of additional diffusion pathways and heterogeneous adsorption domains.

For BC550, the PFO model provided the best fit to the experimental data ($R^2 = 0.993$), with a calculated equilibrium adsorption capacity (18.42 mg/g) very close to the experimental value, whereas the PSO model showed a lower correlation coefficient ($R^2 = 0.964$). In contrast, BC550–5B was better described by the PSO model ($R^2 = 0.988$) instead of the PFO model ($R^2 = 0.978$). The superior performance of the PSO model suggests that adsorption on the composite is governed by stronger interactions between methylene blue molecules and the heterogeneous active sites created by the combined carbonaceous and aluminosilicate phases [4, 33]. These results are consistent with recent studies reporting that pristine biochars frequently exhibit PFO or mixed kinetic behavior, while biochar–bentonite composites tend to follow the PSO model owing to the greater contribution of surface interactions associated with oxygen-containing functional groups, cation-exchange sites, and electrostatic interactions [20, 23]. Although intraparticle diffusion was not evaluated in the present study, the kinetic results, together with the FTIR and XRD analyses, support that adsorption proceeds through the combined contribution of hydrogen bonding, π–π interactions, and electrostatic attraction between methylene blue molecules and the composite surface.

4. CONCLUSIONS

This study systematically evaluated the influence of pyrolysis temperature on the physicochemical, structural, thermal, adsorption equilibrium, and kinetic properties of biochar and biochar–bentonite composites produced from babassu coconut shell (*Attalea speciosa*). Increasing the pyrolysis temperature promoted greater carbonization, aromatic condensation, and thermal stability, while bentonite incorporation enhanced the adsorption performance by introducing additional aluminosilicate active sites. Among the investigated materials, BC550–5B exhibited the best overall performance, reaching a maximum adsorption capacity of 73.89 mg/g. FTIR, XRD, TGA/DTG, SEM/EDS, and elemental mapping demonstrated that the combination of a highly carbonized matrix with a well-dispersed bentonite phase resulted in a structurally stable composite with favorable characteristics for methylene blue adsorption.

Adsorption equilibrium was satisfactorily described by the Langmuir model, indicating predominantly monolayer adsorption on relatively homogeneous active sites, whereas the kinetic analysis revealed distinct adsorption behaviors for the pristine biochar and the composite. BC550 followed the PFO model, while BC550–5B was better represented by the PSO model, suggesting that bentonite incorporation increases the contribution of surface interactions associated with the heterogeneous carbon-clay interface. Overall, the results demonstrate that pyrolysis temperature and mineral modification act synergistically to improve adsorption performance.

The main scientific contribution of this work is the first systematic correlation between pyrolysis temperature, structural evolution, equilibrium behavior, and adsorption kinetics of babassu shell-derived biochar–bentonite composites. Furthermore, the valorization of an abundant Brazilian agro-industrial residue into an efficient, potentially cost-effective adsorbent reinforces the potential of these materials for sustainable

wastewater treatment, circular economy strategies, and biomass waste management. The developed composites therefore show promising adsorption performance under controlled laboratory conditions; however, their practical applicability remains to be established through studies using real textile wastewater, multicomponent systems, continuous-flow operation, regeneration, spent-adsorbent management, and techno-economic assessment.

5. ACKNOWLEDGMENTS

The authors acknowledge Antônio César Honorato Barreto by the FTIR spectra and by physicochemical experiments. This work was supported by CNPq (402757/2023-8, 310037/2023-9); FUNCAP (PS1-00186-00255.01.00/21); CAPES (88887.603218/2021-00); FINEP; and CAPES (Finance Code 001). The financial support provided by the Human Resources Program of the National Petroleum, Natural Gas, and Biofuel Agency – PRH-ANP (PRH 31.1). This support is attained possibly through resources from the investment of qualified oil companies in the P, D&I Clause of ANP Resolution Nº. 50/2015.

6. DATA AVAILABILITY

The complete dataset supporting the results of this study is available upon request from the corresponding author. The dataset is not publicly available due to the presence of potentially identifiable information in some files and the large volume of experimental data.

7. SUPPLEMENTARY MATERIAL

The following online material is available for this article:

Figure A1 – Calibration curve of methylene blue obtained by UV–Vis spectrophotometry at 664 nm. Data points represent the mean values of four independent measurements, and error bars indicate the standard deviation. The solid line corresponds to the linear regression ($y = 0.2348x + 0.0048$; $R^2 = 0.9996$), demonstrating excellent linearity within the concentration range of 0–2.0 mg/L.

Table A1 – List of abbreviations, symbols, and variables used throughout the manuscript.

8. BIBLIOGRAPHY

[1] AL-TOHAMY, R., ALI, S.S., LI, F., *et al*., "A critical review on the treatment of dye-containing wastewater: ecotoxicological and health concerns of textile dyes and possible remediation approaches for environmental safety", *Ecotoxicology and Environmental Safety*, v. 231, pp. 113160, Feb. 2022. doi: https://doi.org/10.1016/j.ecoenv.2021.113160. PubMed PMID: 35026583.

[2] ELGARAHY, A.M., ELWAKEEL, K.Z., MOHAMMAD, S.H., *et al*., "A critical review of biosorption of dyes, heavy metals and metalloids from wastewater as an efficient and green process", *Cleaner Engineering and Technology*, v. 4, pp. 100209, Oct. 2021. doi: https://doi.org/10.1016/j.clet.2021.100209.

[3] CHEN, W.-H., HOANG, A.T., NIŽETIĆ, S., *et al*., "Biomass-derived biochar: from production to application in removing heavy metal-contaminated water", *Process Safety and Environmental Protection*, v. 160, pp. 704–733, Apr. 2022. doi: https://doi.org/10.1016/j.psep.2022.02.061.

[4] COUTINHO DA SILVA, L., SANTIAGO, P.Q., DE SOUSA, E.F., *et al*., "Production and characterization of Carnauba Straw (Copernicia prunifera) Biochar: influence of wax removal on adsorption of methylene blue", *ACS Omega*, v. 11, n. 16, pp. 24522–24535, Apr. 2026. doi: https://doi.org/10.1021/acsomega.6c00684. PubMed PMID: 42077837.

[5] DA SILVA LIMA, P.N., GHOSH, A., NASCIMENTO, A., *et al*., "Advanced sustainable carbon material from babassu biomass and its adsorption performance", *Journal of Physics and Chemistry of Solids*, v. 176, pp. 111188, May. 2023. doi: https://doi.org/10.1016/j.jpcs.2022.111188.

[6] SEWU, D.D., LEE, D.S., TRAN, H.N., *et al*., "Effect of bentonite-mineral co-pyrolysis with macroalgae on physicochemical property and dye uptake capacity of bentonite/biochar composite", *Journal of the Taiwan Institute of Chemical Engineers*, v. 104, pp. 106–113, Nov. 2019. doi: https://doi.org/10.1016/j.jtice.2019.08.017.

[7] HAMAD, H.N., IDRUS, S., YUSUF, B., *et al*., "Optimized bentonite clay adsorbents for methylene blue removal", *Processes (Basel, Switzerland)*, v. 12, n. 4, pp. 738, Apr. 2024. doi: https://doi.org/10.3390/pr12040738.

[8] RAMOLA, S., BELWAL, T., LI, C.J., *et al*., "Improved lead removal from aqueous solution using novel porous bentonite – and calcite-biochar composite", *The Science of the Total Environment*, v. 709, pp. 136171, Mar. 2020. doi: https://doi.org/10.1016/j.scitotenv.2019.136171. PubMed PMID: 31905582.

[9] JANU, R., MRLIK, V., RIBITSCH, D., *et al*., "Biochar surface functional groups as affected by biomass feedstock, biochar composition and pyrolysis temperature", *Carbon Resources Conversion*, v. 4, pp. 36–46, Jan. 2021. doi: https://doi.org/10.1016/j.crcon.2021.01.003.

[10] GAO, L., GOLDFARB, J.L., "Characterization and adsorption applications of composite biochars of clay minerals and biomass", *Environmental Science and Pollution Research International*, v. 28, n. 32, pp. 44277–44287, Aug. 2021. doi: https://doi.org/10.1007/s11356-021-13858-x. PubMed PMID: 33851292.

[11] HARINDINTWALI, J.D., HE, C., XIANG, L., *et al*., "Effects of ball milling on biochar adsorption of contaminants in water: a meta-analysis", *The Science of the Total Environment*, v. 882, pp. 163643, Jul. 2023. doi: https://doi.org/10.1016/j.scitotenv.2023.163643. PubMed PMID: 37086985.

[12] SHAKIR, S.W., AL-YAQOOBI, A.M., "Advanced composite adsorbent based on biochar, bentonite, and boric acid for sustainable removal of Pinoxaden", *International Journal of Renewable Energy Development*, v. 14, n. 6, pp. 1250–1261, Nov. 2025. doi: https://doi.org/10.61435/ijred.2025.61503.

[13] MAPOSSA, A.B., DA SILVA JÚNIOR, A.H., DE OLIVEIRA, C.R.S., *et al*., "Thermal, morphological and mechanical properties of multifunctional composites based on biodegradable polymers/bentonite clay: a review", *Polymers*, v. 15, n. 16, pp. 3443, Aug. 2023. doi: https://doi.org/10.3390/polym15163443. PubMed PMID: 37631500.

[14] YAASHIKAA, P.R., SENTHIL KUMAR, P., KARISHMA, S., "Review on biopolymers and composites – Evolving material as adsorbents in removal of environmental pollutants", *Environmental Research*, v. 212, n. Pt A, pp. 113114, 2022. doi: https://doi.org/10.1016/j.envres.2022.113114. PubMed PMID: 35331699.

[15] CONSIGLIO KASEMODEL, M., ROMÃO, E.L., BUENO RUIZ PAPA, T., "Adsorption of methylene blue on babassu coconut (Orbignya speciosa) mesocarp commercial biochar", *International Journal of Environmental Science and Technology*, v. 21, n. 2, pp. 1671–1682, Jan. 2024. doi: https://doi.org/10.1007/s13762-023-05066-6.

[16] KUANG, Y., ZHANG, X., ZHOU, S., "Adsorption of methylene blue in water onto activated carbon by surfactant modification", *Water (Basel)*, v. 12, n. 2, pp. 587, Feb. 2020. doi: https://doi.org/10.3390/w12020587.

[17] CHANDRASEKAR, R., PRAKASH, P., GHOSH, D., *et al*., "Heteroatom doped biochar-aluminosilicate composite as a green alternative for the removal of hazardous dyes: functional characterization and modeling studies", *Environmental Research*, v. 260, pp. 119579, Nov. 2024. doi: https://doi.org/10.1016/j.envres.2024.119579. PubMed PMID: 38986803.

[18] SANTIAGO, P.Q., SILVA, L.C., SOUSA, E.F., *et al*., "Structural and chemical characterization of carnauba stalk biochar (Copernicia prunifera) and its application in methylene blue adsorption", *Processes (Basel, Switzerland)*, v. 14, n. 6, pp. 905, Mar. 2026. doi: https://doi.org/10.3390/pr14060905.

[19] DING, Z., WAN, Y., HU, X., *et al*., "Sorption of lead and methylene blue onto hickory biochars from different pyrolysis temperatures: importance of physicochemical properties", *Journal of Industrial and Engineering Chemistry*, v. 37, n. 20, pp. 261–267, May. 2016. doi: https://doi.org/10.1016/j.jiec.2016.03.035.

[20] VIEIRA, A.P., SANTANA, S.A.A., BEZERRA, C.W.B., *et al*., "Removal of textile dyes from aqueous solution by babassu coconut epicarp (Orbignya speciosa)", *Chemical Engineering Journal*, v. 173, n. 2, pp. 334–340, Sep. 2011. doi: https://doi.org/10.1016/j.cej.2011.07.043.

[21] NOBRE, J.R.C., QUEIROZ, L.S., CASTRO, J.P., *et al*., "Potential of agro-industrial residues from the Amazon region to produce activated carbon", *Heliyon*, v. 9, n. 7, pp. e17189, Jul. 2023. doi: https://doi.org/10.1016/j.heliyon.2023.e17189. PubMed PMID: 37483770.

[22] KEILUWEIT, M., NICO, P.S., JOHNSON, M.G., *et al*., "Dynamic molecular structure of plant biomass-derived black carbon (Biochar)", *Environmental Science & Technology*, v. 44, n. 4, pp. 1247–1253, Feb. 2010. doi: https://doi.org/10.1021/es9031419. PubMed PMID: 20099810.

[23] RAMESH, K.; RAGHAVAN, V., "Biochar/bentonite composite beads for controlled nitrogen release and reduced environmental impact: from banana waste to sustainable food security", *Results in Surfaces and Interfaces*, v. 19, pp. 100500, May. 2025. doi: https://doi.org/10.1016/j.rsurfi.2025.100500.

[24] AHMAD, M., RAJAPAKSHA, A.U., LIM, J.E., *et al*., "Biochar as a sorbent for contaminant management in soil and water: a review", *Chemosphere*, v. 99, pp. 19–33, Mar. 2014. doi: https://doi.org/10.1016/j.chemosphere.2013.10.071. PubMed PMID: 24289982.

[25] YANG, X., SHAO, X., TONG, J., *et al*., "Removal of aqueous eriochrome blue-black R by novel Na-bentonite/hickory biochar composites", *Separation and Purification Technology*, v. 311, pp. 123209, Apr. 2023. doi: https://doi.org/10.1016/j.seppur.2023.123209.

[26] MAHDI, Z., EL HANANDEH, A., YU, Q., "Influence of pyrolysis conditions on surface characteristics and methylene blue adsorption of biochar derived from date seed biomass", *Waste and Biomass Valorization*, v. 8, n. 6, pp. 2061–2073, Sep. 2017. doi: https://doi.org/10.1007/s12649-016-9714-y.

[27] ANOOP, P.P., PALANISAMY, T., "Coconut shell biochar–Bacillus cereus DKBovi-5 based biocomposite as a sustainable additive for cement mortar: effect of pyrolysis temperature on characterization, strength, hydration, and healing", *Sustainable Chemistry and Pharmacy*, v. 46, pp. 102112, Aug. 2025. doi: https://doi.org/10.1016/j.scp.2025.102112.

[28] WANG, Y., ZHANG, Y., LI, S., *et al*., "Enhanced methylene blue adsorption onto activated reed-derived biochar by tannic acid", *Journal of Molecular Liquids*, v. 268, pp. 658–666, Oct. 2018. doi: https://doi.org/10.1016/j.molliq.2018.07.085.

[29] LIU, R.-L., LIU, Y., ZHOU, X.-Y., *et al*., "Biomass-derived highly porous functional carbon fabricated by using a free-standing template for efficient removal of methylene blue", *Bioresource Technology*, v. 154, n. 11, pp. 138–147, Feb. 2014. doi: https://doi.org/10.1016/j.biortech.2013.12.034. PubMed PMID: 24388956.

[30] BHARDWAJ, A., NAG, S., DAHIYA, A., *et al*., "Effect of pyrolysis temperature on mechanistic transformation for adsorption of methylene blue on leached rice-straw biochar", *Clean (Weinheim)*, v. 50, n. 4, pp. 2100108, Apr. 2022. doi: https://doi.org/10.1002/clen.202100108.

[31] LENG, L., XIONG, Q., YANG, L., *et al*., "An overview on engineering the surface area and porosity of biochar", *The Science of the Total Environment*, v. 763, pp. 144204, Apr. 2021. doi: https://doi.org/10.1016/j.scitotenv.2020.144204. PubMed PMID: 33385838.

[32] VARSHA, M., SENTHIL KUMAR, P., SENTHIL RATHI, B., "A review on recent trends in the removal of emerging contaminants from aquatic environment using low-cost adsorbents", *Chemosphere*, v. 287, n. Pt 3, pp. 132270, Jan. 2022. doi: https://doi.org/10.1016/j.chemosphere.2021.132270. PubMed PMID: 34560497.

[33] ELNOUR, A.Y., ALGHYAMAH, A.A., SHAIKH, H.M., *et al*., "Effect of pyrolysis temperature on biochar microstructural evolution, physicochemical characteristics, and its influence on biochar/polypropylene composites", *Applied Sciences (Basel, Switzerland)*, v. 9, n. 6, pp. 1149, Mar. 2019. doi: https://doi.org/10.3390/app9061149.